JCTC Journal of Chemical Theory and Computation

Article

pubs.acs.org/JCTC

Random Phase Approximation in Surface Chemistry: Water Splitting on Iron

František Karlický, Petr Lazar, Matúš Dubecký, and Michal Otyepka*

Regional Centre of Advanced Technologies and Materials, Department of Physical Chemistry, Palacký University Olomouc, tř. 17. listopadu 12, 771 46 Olomouc, Czech Republic

Supporting Information

ABSTRACT: The reaction of water with zero-valent iron (anaerobic corrosion) is a complex chemical process involving physisorption and chemisorption events. We employ random phase approximation (RPA) along with gradient-corrected and hybrid density functional theory (DFT) functionals to study the reaction of water with the Fe atom and Fe(100) surface. We show that the involvement of the exact electron exchange and nonlocal correlation effects in RPA improves the description of all steps of the reaction on the Fe surface with respect to standard [meaning local density approximation (LDA) or generalized gradient approximation (GGA)] DFT methods. The reaction profile calculated by range-separated hybrid functional HSE06 agrees reasonably well with the RPA profile, which makes HSE06 a computationally less demanding alternative to RPA. We also investigate the reaction of the Fe atom with water using DFT, RPA, and coupled-cluster through the perturbative triples complete basis set [CCSD(T)-3*s*3*p*-DKH/CBS] method. Local DFT methods significantly underestimate reaction barriers, while the reaction kinetics and thermodynamics from RPA agree with the reference CCSD(T) data. Both systems, i.e., the Fe atom and Fe(100), provide the same reaction mechanism, indicating that anaerobic corrosion is a stepwise process involving one-electron steps, with the first reaction step (formation of the HFeOH intermediate) representing the rate-limiting step.

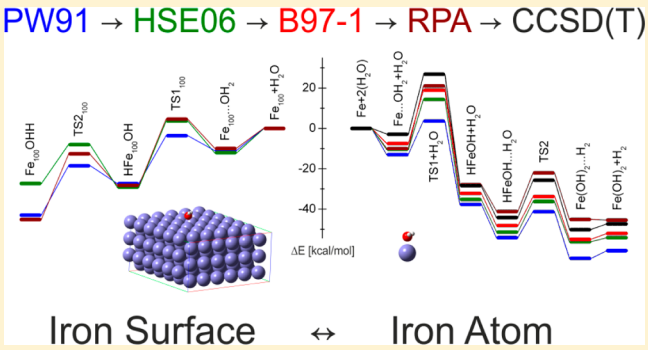

INTRODUCTION

Physisorption, chemisorption, and catalysis on solid surfaces have been widely studied over many decades and still attract interest because of their fundamental importance in surface chemistry.[1−4] Theoretical calculations of these processes usually utilize density functional theory (DFT),[5,6] which can be effectively formulated under periodic boundary conditions. However, widely used classical DFT functionals, i.e., local density approximation (LDA) and generalized gradient approximation (GGA), are impaired by inherent limitations.[7,8] The self-interaction error (SIE) and the neglect of nonlocal electron correlation effects are two of the most serious limitations in using these functionals to model molecule−surface interactions and processes. Thus, adsorption energies and reaction barriers for such systems cannot yet be calculated with chemical accuracy.[9−11]

Various methods have been developed to overcome the shortcomings of classical DFT functionals. The SIE can be effectively reduced by using hybrid DFT functionals involving some portion of the exact Hartree−Fock exchange; moreover, short-range functionals, such as screened hybrid functional HSE06,[12] seem to be an effective alternative for periodic systems.[13−15] Nonlocal correlations pose a more difficult problem. Nevertheless, in recent years, an ever-growing toolbox of theoretical approaches has been developed to incorporate the nonlocal electron correlations into the DFT framework. Grimme[16] and Jurečka[17] used an empirical pairwise potential as a dispersion correction, and this simple solution inspired more elaborate approaches.[18] An important step forward was the development of an approximate nonlocal density functional (vdW-DF).[19] However, vdW-DF is very sensitive to the choice of the exchange part.[20−22]

The random phase approximation (RPA)[23−25] to the correlation energy represents another advance. It naturally includes van der Waals interactions with the correct asymptotic decay. Besides the improved description of bulk material properties,[26] RPA corrects the tendencies of local density functionals, like underestimation of surface energies and/or overestimation of chemisorption energies.[27,28] However, assessment of its performance for surface reactions is hampered by the lack of accurate benchmark energies or experimental data, together with the high computational costs of the RPA in the case of surface calculations.

In this work, we investigate the reaction of water with zero-valent iron, which plays the key role in processes such as anaerobic corrosion and water remediation by zero-valent iron (nano)particles.[29,30] Here we focus on the initial steps of the

Received: May 23, 2013
Published: July 10, 2013

   dx.doi.org/10.1021/ct400425p | J. Chem. Theory Comput. 2013, 9, 3670−3676

anaerobic corrosion process. The challenge for theoretical calculations lies in the fact that the reaction involves physisorption, chemical changes, and a transition metal. Two systems are analyzed: (i) the first one being the reaction of the iron atom with water [$Fe + 2H_2O \rightarrow Fe(OH)_2 + H_2$] and (ii) the other describing the reaction of a water molecule with the large model of the Fe(100) surface. The relatively small size of the atomic system allowed the use of advanced quantum chemical methods. We identified important stationary points on the reaction pathway and calculated their energies by the coupled cluster method expanded to perturbative triples, CCSD(T), including scalar relativity [using the Douglas–Kroll–Hess method (DKH)] and valence plus outer-core (3*s*3*p*) electronic correlations followed by extrapolation of the total energies to the complete basis set (CBS) limit (see Methods for details). CCSD(T)-3*s*3*p*-DKH/CBS allowed consistent and reliable treatment of the reaction of water with zero-valent iron[31] at a thermochemical accuracy for transition metals, i.e., error in energies of <3 kcal/mol.[32] Several DFT functionals [GGA (PW91),[33] short-range hybrid (HSE06),[12] and hybrid (B97-1)[34]] and the (RPA+EX)@PBE method were benchmarked against the CCSD(T)-3*s*3*p*-DKH/CBS results to assess their accuracy for subsequent use in surface calculations. Finally, we employed DFT and RPA calculations for the dissociation of the water molecule on the 3 × 3 model of the Fe(100) surface. We provide, for the first time to the best of our knowledge, the energies of RPA quality for the reaction on the periodic surface of a solid and utilize the results to discuss the functionals, their flaws and limitations, in the general context of surface chemistry.

METHODS

Initial geometry optimizations for the $Fe + 2H_2O$ reaction were performed using unrestricted density functional theory, employing the B97-1,[34] HSE06,[12] and PW91[33] functionals in conjunction with cc-pVTZ basis sets for hydrogen,[35] oxygen,[35] and iron.[36] The Gibbs free energy (ΔG) was obtained by adding zero-point vibrational energy (ZPE) corrections and Gibbs energy corrections calculated within harmonic approximation using the B97-1 functional to the corresponding electronic energy (ΔE). The nature of all identified stationary points on the potential energy surface (PES) was tested by examining the eigenvalues of the Hessian matrix, and the intrinsic reaction coordinate method was used to verify the correspondence of transition structures to their adjacent minima. Subsequent single-point energy calculations on B97-1 geometries employed the unrestricted CCSD(T) theory, including scalar relativistic effects (using the DKH method of the second order) and valence plus outer-core (3*s*3*p*) electronic correlations [denoted CCSD(T)-3*s*3*p*-DKH below] followed by extrapolation of the total energies to the complete basis set (CBS) limit from bases of triple-ζ and quadruple-ζ cardinalities (cc-pwCV*n*Z-DK for iron,[36] where n = 3 or 4). Final single-point DFT energies were obtained using cc-pVQZ basis sets. All calculations were performed using the Gaussian suite of programs.[37] The reliability of the scheme used for the electronic structure calculations of iron–water complexes has been extensively tested in our previous work.[31,38]

RPA can be derived from various theoretical frameworks. The original formulation[23−25] was one of several approximations employed to treat oscillations and excitations in the homogeneous electron gas. It can be formulated from the perspective of many-body perturbation theory and has been introduced into the framework of DFT via the so-called adiabatic connection fluctuation dissipation theorem. The background and various formulations of RPA have been presented in great detail in excellent recent reviews.[39,40]

The RPA calculations were performed using the plane-wave (PW) VASP code.[41,42] The RPA calculation can be, in principle, performed self-consistently; however, because of enormous computational demands of such calculation, RPA and exact exchange (EX) were evaluated on top of the Kohn–Sham DFT orbitals determined using the Perdew–Burke–Ernzerhof (PBE)[43] functional [(RPA+EX)@PBE in the text]. Different computational setups were used for the RPA and EX calculations on the atomic system. (1) Reacting species with B97-1 geometries were placed in a cubic cell with a side length of 10 Å, and the RPA energy was calculated with an energy cutoff E_{cut} of 375 eV. (2) The EX energy was evaluated with an E_{cut} of 400 eV, and the size of the cell was increased to 20 Å to separate the long-range tails of the Fock exchange. Spin polarization was taken into account in all calculations, and spin densities were allowed to relax.

The Fe(100) surface was modeled by a 3 × 3 periodic slab model. The slab contained three atomic layers (i.e., 27 iron atoms) separated by 8 Å of vacuum. The geometries of important reaction steps were taken from our previous study.[44] The energy cutoff of 350 eV was utilized, as this value provided convergent total energies (see the Supporting Information for cutoff convergence). The Brillouin zone was sampled by the 3 × 3 × 1 k-point mesh [in addition, 2 × 2 × 1 mesh was used for testing purposes (see the Supporting Information)] for the RPA calculations on the surface. In the case of surface calculation, the exchange energy EX was evaluated with the same computational setup (cutoff, k-points) as each RPA energy, because this procedure provided the fastest convergence for bulk metals.[26] It should be noted that RPA calculations on this relatively large molecule–surface system are on the very edge of today's computational capabilities, requiring ∼10 GB of memory per central processing unit core and long computational times even on modern computer clusters. The RPA:HSE06:GGA ratio of relative computational costs for single-point surface calculations using those functionals can be roughly estimated to be 100:10:1.

RESULTS AND DISCUSSION

Reaction with the Fe Atom: Reaction Mechanism. The reaction of water with an iron atom is a stepwise process initiated by physisorption, followed by a chemical change (Figure 1). The potential energy surface of the $Fe + 2H_2O$ system was extensively searched for stationary points, and we identified the most probable reaction path from the thermodynamic perspective, i.e., the path through two transition states, TS1 and TS2, finishing with the products $Fe(OH)_2$ and H_2 (Figure 1). In addition, we examined many alternative pathways [e.g., through complexes $Fe + (H_2O)_2$, $H_2O\cdots Fe\cdots OH_2$, and $TS1\cdots OH_2$ or to other products such as FeO, H_2, and H_2O or FeOH, H, and H_2O] that were not energetically competitive with respect to the reported minimal energy reaction path (these pathways are not further discussed for the sake of brevity). To verify that the ground electronic state of the reaction coordinate retained the quintet multiplicity and that no spin crossing occurred, we also performed calculations for triplet multiplicity. For all stationary points on the PES of the $Fe + 2H_2O \rightarrow Fe(OH)_2 + H_2$ reaction, the quintet state was favorable at the CCSD(T)-3*s*3*p*-DKH/CBS

dx.doi.org/10.1021/ct400425p | J. Chem. Theory Comput. 2013, 9, 3670−3676

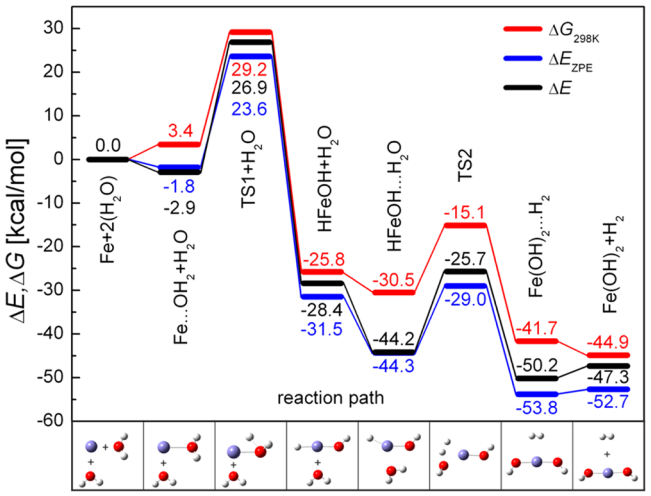

Figure 1. Reaction scheme showing the quintet $Fe^0 + 2H_2O$ reaction path in the gas phase (red) at the CCSD(T)-3*s*3*p*-DKH/CBS level. Minimal energy paths excluding (black) and including (blue) zero-point energy are added for comparison. The plus sign denotes infinite separation of the complex. Energies of the first four compounds were adopted from ref 31.

level by at least 25 kcal/mol. This finding was also confirmed by the independent spin-polarized single-point PBE/PW calculation (used later for RPA) with a relaxed magnetic moment.

The reaction begins as the H_2O molecule approaches the Fe atom (^5D, $3d^64s^2$) and forms a noncovalent Fe···OH_2 complex (Figure 1) with nonplanar geometry and C_s symmetry. The reaction proceeds by migration of one of the hydrogen atoms to form the highly stable planar nonlinear HFeOH intermediate state with effective electronic atomic configurations H($1s^{1.5}$)-Fe($4s^{0.5}3d^{6.2}4p^{0.2}$)-O($2s^{1.8}2p^{5.3}$)-H($1s^{0.5}$) via transition state TS1 [Fe($4s^{1.1}3d^{6.4}4p^{0.1}$)-H($1s^{0.9}$)-O($2s^{1.8}2p^{5.2}$)-H($1s^{0.5}$)]. The barrier height for this process ($\Delta G^{\ddagger}_{298\ K}$) is 29.2 kcal/mol in the gas phase. From Fe···OH_2 to TS1, the FeOH angle is reduced from 109.8° to 57.0° and the hydrogen atom from the oxygen side of the molecule is shifted to a position above the Fe−O bond. The OH distance increases to 1.47 Å, while a new Fe−H bond (1.65 Å) starts to form. The long Fe−O bond of 2.17 Å in the Fe···OH_2 complex is shortened to 1.79 Å in HFeOH (cf. with 1.60 Å in FeO). It should be noted that the existence of the HFeOH molecule was experimentally demonstrated by argon matrix isolation Fourier transform infrared spectroscopy.[45,46] The second water molecule then joins HFeOH, forming a noncovalent HFeOH···H_2O complex with an almost planar geometry, the only exception being the remote H atom of the second water molecule (Figure 1). The reaction continues by rotation of the second water molecule and migration of one hydrogen atom via transition state TS2 (Figure 1) to form a highly symmetric (C_{2v} symmetry) complex, Fe(OH)$_2$···H_2, which spontaneously breaks into a free Fe(OH)$_2$ and hydrogen. The barrier height for the second step of the reaction ($\Delta G^{\ddagger}_{298\ K}$), evolving via transition state TS2, is 15.3 kcal/mol. From HFeOH···H_2O to TS2, the OFeO angle is increased from 80.6° to 146.8° and the hydrogen atoms from both oxygen and iron sites of the HFeOH···H_2O complex are shifted to elevated positions above the newly formed Fe−O bond [1.99 Å (see Figure 1)]. Finally, the O−Fe−O angle 176.0° in Fe(OH)$_2$···H_2 is similar to the O−Fe−O angle in the product [Fe(OH)$_2$, 176.7°], while the symmetry of the product (C_2, H−O−O−H dihedral angle of 88.9°) is lower with respect to planar Fe(OH)$_2$···H_2 (C_{2v}). For Fe(OH)$_2$, an analysis of the natural orbitals provides the effective electronic atomic configurations Fe($4s^{0.3}3d^{6.3}4p^{0.2}$)-2O($2s^{1.8}2p^{5.3}$)-2H($1s^{0.5}$). The analysis of the natural orbitals and geometrical parameters provided in this section were obtained on the B97-1/cc-pVTZ level; for complete effective configurations from various methods, together with effective charges, see Table S1 of the Supporting Information.

To summarize this part, the CCSD(T)-3*s*3*p*-DKH/CBS free energy profiles showed two separated reaction steps (Figure 1): $Fe^0 + H_2O \rightarrow HFe^{I}OH$, followed by $HFe^{I}OH + H_2O \rightarrow Fe^{II}(OH)_2 + H_2$. Both steps represented single-electron steps, as the oxidation number of iron gradually increased by one. The first reaction step, i.e., splitting of the H−OH bond of water and formation of the HFeOH molecule, was the rate-limiting step with a corresponding reaction barrier ($\Delta G^{\ddagger}_{298\ K}$ = 29.2 kcal/mol) almost 2 times higher than the activation barrier of the second step, which leads to the production of Fe(OH)$_2$ and hydrogen. It is worth noting that zero-point vibrations only weakly influenced the energies (Figure 1). The effect of entropy was more pronounced, because of the suppression of the degrees of freedom in the transition from the two-component system (e.g., HFeOH + H_2O) to the one-component system (HFeOH···H_2O).

Reaction with the Fe Atom: Comparison of Potential Energy Surfaces from Various Methods. To assess the accuracy of GGA (PBE), short-range hybrid (HSE06), hybrid (B97-1), and (RPA+EX)@PBE methods, we compared the reaction profiles from those methods against the CCSD(T)-3*s*3*p*-DKH/CBS profile for the Fe + $2H_2O \rightarrow$ Fe(OH)$_2$ + H_2 reaction in which the relatively small size of the atomic system allowed the use of advanced quantum chemical methods. For such purposes, we used pure potential energies (ΔE) without any entropy corrections to provide unbiased comparisons of the methods. There are two partial limitations of the methods used for evaluating the Fe + $2H_2O$ reaction. The first possible source of small errors in total energies could arise from the DFT geometries used in high-level wave function-based calculations. In principle, DFT stationary points on the PES do not necessarily correspond to stationary points on the CCSD(T)-3*s*3*p*-DKH or (RPA+EX)@PBE level, which may lead to a bias in the computed properties such as dissociation energies or reaction barriers. In our previous work,[31,38] we conducted some optimizations of geometries using a broader set of density functionals and the CCSD method. The B97-1 density functional gave the most similar geometries with respect to computationally demanding CCSD optimizations, and hence, we use B97-1 geometries for subsequent CCSD(T) and (RPA+EX)@PBE calculations. It should be noted that our previous calculations for iron−water complexes showed rather flat PES. We may therefore assume that possible errors resulting from the use of DFT geometries are not critical. The other bias in total energy calculations could arise from a possible multireference character of the species studied. Utilization of unrestricted methods may result in the admixture of higher spin states in the excited configurations, and the results may thus be perturbed by spin contamination. However, the coupled cluster methods [especially CCSD(T)] are quite efficient at reducing UHF spin contamination to acceptable levels.[47] As a control, not only the spin contaminations but also single-excitation amplitudes in a coupled cluster expansion and T_1 diagnostics were all monitored (Table 1), taking into account that a T_1 diagnostic of >0.05 usually indicates some

dx.doi.org/10.1021/ct400425p | J. Chem. Theory Comput. 2013, 9, 3670−3676

Table 1. T_1 Diagnostics, Largest Single-Excitation Amplitudes (A_{max}) in Coupled Cluster Expansion, and Numbers (N_a) of Amplitudes Greater Than 0.1[a]

	T_1	A_{max}	N_a
Fe	0.019	0.007	0
Fe···OH_2	0.042	0.132	2
TS1	0.046	0.119	1
HFeOH	0.022	0.007	0
HFeOH···H_2O	0.058	0.281	8
TS3	0.034	0.140	2
$Fe(OH)_2$···H_2	0.021	0.009	0
$Fe(OH)_2$	0.021	0.006	0

[a]All values shown are for the CCSD(T)-3*s*3*p*-DKH/cc-pwCVQZ-DK calculation.

multireference character of the wave function.[48] In our case, the only problematic species (despite very little spin contamination) is HFeOH···H_2O with a T_1 of 0.058 due to several enlarged amplitudes (further details on spin contaminations can be found in Table S3 of the Supporting Information). Notwithstanding these limitations, we believe that the global view of the energetics of the Fe + $2H_2O$ → $Fe(OH)_2$ + H_2 reaction under study is rather unbiased, which is also demonstrated by comparison of the computed thermochemistry of several complexes with the salient data available in the literature (see our previous work[31,38]).

The potential energy surfaces of the Fe + $2H_2O$ → $Fe(OH)_2$ + H_2 reaction (Figure 2) clearly show that despite the fact that

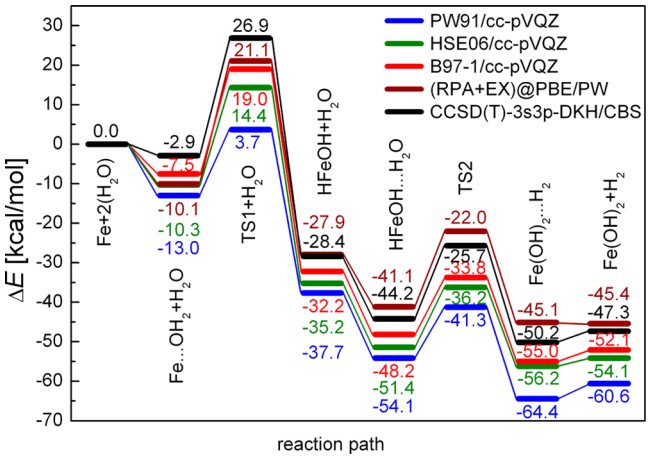

Figure 2. Minimal energy path of the Fe^0 + $2H_2O$ reaction scheme calculated using various methods.

GGA functional (PW91) provides adequate results for the species in potential energy minima, it strongly underestimates both activation barriers (16.7 and 12.8 kcal/mol for TS1 and TS2, respectively). Hybrid functionals, HSE06 and B97-1, systematically improve the dissociation barrier heights and the reaction thermodynamics but still underestimate the energies of the transition states with respect to the reference CCSD(T)-3*s*3*p*-DKH/CBS data. The (RPA+EX)@PBE energies in Figure 2 show further improvement versus those of both hybrid functionals. The (RPA+EX)@PBE activation barrier of 31.1 kcal/mol for the first dissociation fits well with the value of 29.7 kcal/mol obtained by the CCSD(T)-3*s*3*p*-DKH/CBS method. Similarly, (RPA+EX)@PBE successfully captures the energies of the second transition state, TS2 [barriers of 19.1 and 18.5 kcal/mol at (RPA+EX)@PBE and CCSD(T)-3*s*3*p*-DKH/CBS levels, respectively], and provides a balanced description of the reaction thermodynamics overall.

The failure of the GGA functional stems predominantly from the self-interaction error, which is the most pronounced for open-shell d or f electrons, or for any stretched bonds over which electrons are shared. Stretched bonds indeed occur at the transition states, and utilizing the self-interaction correction method (denoted usually as SIC or SIC-GGA), the energy barriers to chemical reactions in molecular systems were improved significantly versus those from local functionals.[49,50] Thus, an improved description of the transition states may be largely attributed to the exact exchange used in connection with RPA. The exact exchange energy partially cancels the self-interaction error present in the Hartree−Fock term of local functionals. The reaction profile calculated by the hybrid functional corroborates this hypothesis; HSE06 incorporates one-quarter of exact exchange, and therefore, the self-interaction error is reduced. As a result, the HSE06 functional improves the dissociation barrier heights and the reaction thermodynamics versus those of PBE but still fails to meet the energies of the transition states given by the CCSD(T)-3*s*3*p*-DKH/CBS method.

It should be noted that the sole exact exchange would not be sufficient. The Hartree−Fock method typically predicts overly high energies for delocalized charge distributions in transition states,[8] resulting in overestimated reaction barriers. Our calculation corroborates this tendency; sole exact exchange would yield activation barriers as high as 50.8 and 35.0 kcal/mol for TS1 and TS2, respectively. The correlation energy, here approximated by RPA, is clearly necessary to counterbalance this tendency. A slight deviation with respect to CCSD(T) appears only for the initial noncovalent Fe···H_2O complex, for which (RPA+EX)@PBE predicts a binding energy of 10.1 kcal/mol, whereas CCSD(T)-3*s*3*p*-DKH/CBS finds very weak noncovalent bonding (2.9 kcal/mol). Gradient-corrected and hybrid DFT functionals yield binding energies very similar to that provided by RPA. This might be due to the improper description of free standing atoms with a degenerate ground state within the DFT approach.[51]

Reaction on the Fe Surface. Next, we compare standard DFT against RPA for the water dissociation reaction on the Fe(100) surface. On the Fe(100) surface, the water molecule adsorbs as the molecular precursor state and decomposes into the OH and H surface-bound species.[44,52] The (RPA+EX)@PBE energies of the reagent (adsorbed H_2O) and the product ($HFe_{100}OH$ in Figure 3) are similar to those calculated by the GGA or HSE06 functional, except for the final product ($Fe_{100}OHH$ in Figure 3), for which HSE06 produces an overly high adsorption energy with respect to those of other methods. The energies of the transition states in the (RPA+EX)@PBE calculation do not increase significantly over the HSE06 results. The first dissociation barrier on the surface has a value of 14.6 kcal/mol, i.e., significantly lower than the value obtained for the atomic system (31.1 kcal/mol). The calculations also corroborate the fact that local functionals (such as LDA or PBE) predict overly low energies for transition states, resulting in underestimated reaction barriers, even for extended systems such as metal surfaces. The reaction profile from RPA is consistent with the results of the experimental study of the oxidation of Fe(100) by water adsorption,[53] which indicates that the dissociation of water into adsorbed hydroxyl and hydrogen starts after some of the water molecules are desorbed

dx.doi.org/10.1021/ct400425p | J. Chem. Theory Comput. 2013, 9, 3670−3676

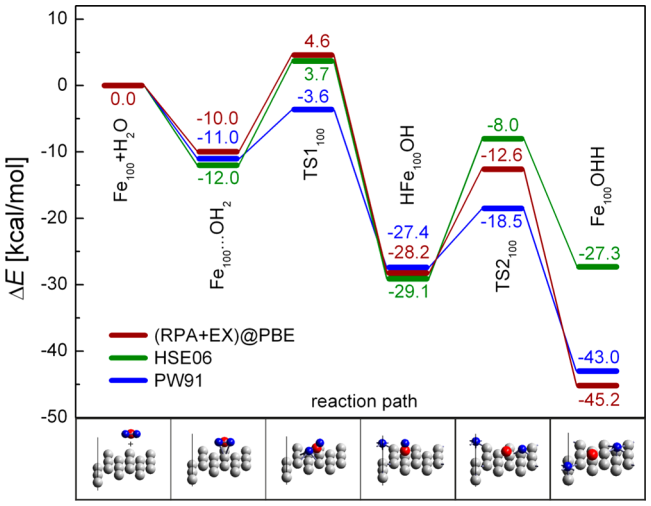

Figure 3. Reaction scheme showing the minimal energy path of the reaction of the water molecule on the Fe(100) surface obtained using the (RPA+EX)@PBE method. The geometries (PW91) and the PW91 and HSE06 energies (calculated using a 3 × 3 × 1 k-point grid and an energy cutoff of 400 eV) are reproduced from ref 44 and are displayed for comparison.

from the surface, and that higher temperatures are needed to disproportionate the hydroxyl overlayer.

Using these results, we can discuss the functionals in a more general context of surface chemistry. The first issue is that gradient-corrected local functionals generally tend to underestimate surface energies and, in fact, predict surfaces are more stable than they really are.[54,55] Hybrid functionals offer only little help in curing this tendency.[56] RPA, on the other hand, provided the surface energies of Pt(111) and Rh(111) in reasonable agreement with experiment.[27] The second issue is that the gradient-corrected functionals overestimate the adsorption energies of covalently bonded species,[27] mainly because they predict stronger hybridization by placing unoccupied molecular orbitals too close to the Fermi level. That seems not to be the case in our study, because the adsorption energy of the H_2O molecule on the iron surface from the GGA functional (−11.0 kcal/mol) is only slightly increased in the (RPA+EX)@PBE calculation (−10.0 kcal/mol). However, this agreement can be a consequence of fortuitous error cancellation in GGA, because the strong hybridization may be compensated by the lack of dispersion interaction, which is entirely ignored by the GGA functional.

The most crucial deficiency of the gradient-corrected functional appears when we inspect the transition states. Both the hybrid functional and the (RPA+EX)@PBE method increase the energies of transition states so that activation barriers are twice as high as those calculated by GGA. Such changes would lead to completely different surface chemistry, because reaction rates depend exponentially on the activation energy. The failure of the GGA functional stems predominantly from the self-interaction error, which is large for stretched bonds occurring at transition states. Thus, an improved description of transition states by (RPA+EX)@PBE may be attributed to the usage of the exact exchange, which is free of self-interaction. Via comparison of the transition states on the iron surface and the atom, the energy difference between GGA and (RPA+EX)@PBE is pronouncedly reduced on the surface. The self-interaction error is less severe for predominantly disperse states on the Fe surface, with respect to the localized states of the atom. Notice also that the height of the barrier itself is much lower on the surface, while the adsorption energy of the H_2O molecule is very similar to that of the atomic model. The water molecule adsorbs on top of one of the Fe atoms on the surface. Therefore, its adsorption geometry is similar to the position found for the atomic model. The transition state (the first dissociation barrier) on the surface on the other hand differs, because the dissociated hydrogen atom interacts with neighboring Fe atoms (see the geometries in Figure 3).

CONCLUSIONS

In conclusion, we investigated the physisorption and chemical reaction of water with iron using two systems, the Fe atom and the Fe(100)−(3 × 3) surface. The size of the atomic system allowed us to use CCSD(T)-3*s*3*p*-DKH/CBS as a benchmark method. The reaction of two water molecules with the iron atom proceeds over two separated reaction barriers, $Fe^0 + H_2O \rightarrow HFe^{I}OH$ followed by $HFe^{I}OH + H_2O \rightarrow Fe^{II}(OH)_2 + H_2$. The first reaction step, i.e., the splitting of the H−OH bond and the formation of the HFeOH molecule, represents the rate-limiting step ($\Delta G^{\ddagger}_{298\ K} \sim 29$ kcal/mol). We compared data from various DFT functionals and the RPA method with the CCSD(T)-3*s*3*p*-DKH/CBS data and observed the following systematic increase in the accuracy of the density functionals: generalized gradient → hybrid → random phase approximation [with the third one providing an improved agreement with the CCSD(T)-3*s*3*p*-DKH/CBS reaction profile]. We further evaluated RPA energies for water dissociation on the Fe(100) surface. The barrier (from RPA) was significantly lower than that obtained in the reaction with the Fe atom. The results reveal that local functionals vastly underestimate activation barriers even for less localized states of metallic solid: the barrier height calculated by (RPA+EX)@PBE was found to be 14.6 kcal/mol, whereas a value of 7.4 kcal/mol was obtained from the PW91 functional. Our findings indicate that great care must be taken when modeling a phenomenon such as catalysis or dissociation using (semi)local DFT functionals. The RPA approach provides a physically correct description of adsorption and systematically improved reaction barriers, in addition to previously reported improvement of bulk and surface properties of solids.[26,27,57] Considering that RPA can be systematically improved by including, for instance, second-order exchange diagrams,[58] single excitations,[59] frequency-dependent exact exchange,[60] or renormalized adiabatic kernels,[61] it offers a way beyond local density approximations and can become an accurate and versatile method in surface chemistry and physics. Range-separated hybrid functional HSE06 can, on the other hand, be recommended as a computationally less demanding alternative to RPA, because of the good correspondence of the reaction profiles calculated by both methods.

ASSOCIATED CONTENT

Supporting Information

Additional details of the calculation of the RPA energy, effective charge, and electronic configurations (Table S1) for all points on the Fe + $2H_2O$ reaction path, spin contaminations (Table S2), free energy profiles for several additional computational methods (Figure S1), convergence tests of (RPA+EX)@PBE energy profiles for the H_2O + Fe(100) surface reaction, and Cartesian coordinates for all points on the Fe + $2H_2O$ reaction path. This material is available free of charge via the Internet at http://pubs.acs.org.

AUTHOR INFORMATION

Corresponding Author

*E-mail: michal.otyepka@upol.cz.

Author Contributions

F.K. and P.L. contributed equally to this work.

Notes

The authors declare no competing financial interest.

ACKNOWLEDGMENTS

Financial support from the Czech Science Foundation (Grants GACR P208/11/P463 and P208/12/G016), the Operational Program Research and Development for Innovations-European Regional Development Fund (Project CZ.1.05/2.1.00/03.0058, Ministry of Education, Youth and Sports of the Czech Republic), the Technology Agency of the Czech Republic ("Competence Centres", Project TE01010218), and the Operational Program Education for Competitiveness-European Social Fund (Projects CZ.1.07/2.3.00/20.0017 and CZ.1.07/2.3.00/30.0004, Ministry of Education, Youth and Sports of the Czech Republic) is gratefully acknowledged. Surface calculations were, in part, performed at the Computing Centre of the Slovak Academy of Sciences, using the supercomputing infrastructure acquired in Projects ITMS 26210120002 and 26230120002 (Slovak infrastructure for high-performance computing) supported by Operational Programme Research and Development funded by the ERDF.

REFERENCES

(1) Carrasco, J.; Hodgson, A.; Michaelides, A. A Molecular Perspective of Water at Metal Interfaces. *Nat. Mater.* **2012**, *11*, 667−674.

(2) Aradhya, S. V.; Frei, M.; Hybertsen, M. S.; Venkataraman, L. Van der Waals Interactions at Metal/Organic Interfaces at the Single-Molecule Level. *Nat. Mater.* **2012**, *11*, 872−876.

(3) Ding, F.; Yakobson, B. Challenges in Hydrogen Adsorptions: From Physisorption to Chemisorption. *Front. Phys.* **2011**, *6*, 142−150.

(4) Weiss, W.; Ranke, W. Surface Chemistry and Catalysis on Well-Defined Epitaxial Iron-Oxide Layers. *Prog. Surf. Sci.* **2002**, *70*, 1−151.

(5) Hohenberg, P.; Kohn, W. Inhomogeneous Electron Gas. *Phys. Rev. B* **1964**, *136*, B864−B871.

(6) Kohn, W.; Sham, L. J. Self-Consistent Equations Including Exchange and Correlation Effects. *Phys. Rev.* **1965**, *140*, A1133−A1138.

(7) Burke, K. Perspective on Density Functional Theory. *J. Chem. Phys.* **2012**, *136*, 150901.

(8) Cohen, A. J.; Mori-Sanchez, P.; Yang, W. T. Challenges for Density Functional Theory. *Chem. Rev.* **2012**, *112*, 289−320.

(9) Díaz, C.; Pijper, E.; Olsen, R. A.; Busnengo, H. F.; Auerbach, D. J.; Kroes, G. J. Chemically Accurate Simulation of a Prototypical Surface Reaction: H_2 Dissociation on Cu(111). *Science* **2009**, *326*, 832−834.

(10) Nørskov, J. K.; Abild-Pedersen, F.; Studt, F.; Bligaard, T. Density Functional Theory in Surface Chemistry and Catalysis. *Proc. Natl. Acad. Sci. U.S.A.* **2011**, *108*, 937−943.

(11) Lazar, P.; Karlický, F.; Jurečka, P.; Kocman, M.; Otyepková, E.; šafářová, K.; Otyepka, M. Adsorption of Small Organic Molecules on Graphene. *J. Am. Chem. Soc.* **2013**, *135*, 6372−6377.

(12) Krukau, A. V.; Vydrov, O. A.; Izmaylov, A. F.; Scuseria, G. E. Influence of the Exchange Screening Parameter on the Performance of Screened Hybrid Functionals. *J. Chem. Phys.* **2006**, *125*, 224106.

(13) Heyd, J.; Peralta, J. E.; Scuseria, G. E.; Martin, R. L. Energy Band Gaps and Lattice Parameters Evaluated with the Heyd-Scuseria-Ernzerhof Screened Hybrid Functional. *J. Chem. Phys.* **2005**, *123*, 174101.

(14) Barone, V.; Hod, O.; Peralta, J. E.; Scuseria, G. E. Accurate Prediction of the Electronic Properties of Low-Dimensional Graphene Derivatives Using a Screened Hybrid Density Functional. *Acc. Chem. Res.* **2011**, *44*, 269−279.

(15) Karlicky, F.; Zboril, R.; Otyepka, M. Band Gaps and Structural Properties of Graphene Halides and Their Derivates: A Hybrid Functional Study with Localized Orbital Basis Sets. *J. Chem. Phys.* **2012**, *137*, 034709.

(16) Grimme, S. Semiempirical GGA-type Density Functional Constructed with a Long-Range Dispersion Correction. *J. Comput. Chem.* **2006**, *27*, 1787−1799.

(17) Jurecka, P.; Cerny, J.; Hobza, P.; Salahub, D. R. Density Functional Theory Augmented with an Empirical Dispersion Term. Interaction Energies and Geometries of 80 Noncovalent Complexes Compared with Ab Initio Quantum Mechanics Calculations. *J. Comput. Chem.* **2007**, *28*, 555−569.

(18) Tkatchenko, A.; Scheffler, M. Accurate Molecular Van Der Waals Interactions from Ground-State Electron Density and Free-Atom Reference Data. *Phys. Rev. Lett.* **2009**, *102*, 073005.

(19) Dion, M.; Rydberg, H.; Schroder, E.; Langreth, D. C.; Lundqvist, B. I. Van der Waals Density Functional for General Geometries. *Phys. Rev. Lett.* **2004**, *92*, 246401.

(20) Klimes, J.; Bowler, D. R.; Michaelides, A. Van der Waals Density Functionals Applied to Solids. *Phys. Rev. B* **2011**, *83*, 195131.

(21) Granatier, J.; Lazar, P.; Otyepka, M.; Hobza, P. The Nature of the Binding of Au, Ag, and Pd to Benzene, Coronene, and Graphene: From Benchmark CCSD(T) Calculations to Plane-Wave DFT Calculations. *J. Chem. Theory Comput.* **2011**, *7*, 3743−3755.

(22) Granatier, J.; Lazar, P.; Prucek, R.; Safarova, K.; Zboril, R.; Otyepka, M.; Hobza, P. Interaction of Graphene and Arenes with Noble Metals. *J. Phys. Chem. C* **2012**, *116*, 14151−14162.

(23) Bohm, D.; Pines, D. A Collective Description of Electron Interactions. I. Magnetic Interactions. *Phys. Rev.* **1951**, *82*, 625−634.

(24) Pines, D.; Bohm, D. A Collective Description of Electron Interactions: II. Collective vs Individual Particle Aspects of the Interactions. *Phys. Rev.* **1952**, *85*, 338−353.

(25) Bohm, D.; Pines, D. A Collective Description of Electron Interactions: III. Coulomb Interactions in a Degenerate Electron Gas. *Phys. Rev.* **1953**, *92*, 609−625.

(26) Harl, J.; Schimka, L.; Kresse, G. Assessing the Quality of the Random Phase Approximation for Lattice Constants and Atomization Energies of Solids. *Phys. Rev. B* **2010**, *81*, 115126.

(27) Schimka, L.; Harl, J.; Stroppa, A.; Gruneis, A.; Marsman, M.; Mittendorfer, F.; Kresse, G. Accurate Surface and Adsorption Energies From Many-Body Perturbation Theory. *Nat. Mater.* **2010**, *9*, 741−744.

(28) Paier, J.; Ren, X.; Rinke, P.; Scuseria, G. E.; Gruneis, A.; Kresse, G.; Scheffler, M. Assessment of Correlation Energies Based on the Random-Phase Approximation. *New J. Phys.* **2012**, *14*, 043002.

(29) Li, L.; Fan, M. H.; Brown, R. C.; Van Leeuwen, J. H.; Wang, J. J.; Wang, W. H.; Song, Y. H.; Zhang, P. Y. Synthesis, Properties, and Environmental Applications of Nanoscale Iron-Based Materials: A Review. *Crit. Rev. Environ. Sci. Technol.* **2006**, *36*, 405−431.

(30) Tratnyek, P. G.; Johnson, R. L. Nanotechnologies for Environmental Cleanup. *Nano Today* **2006**, *1*, 44−48.

(31) Karlicky, F.; Otyepka, M. First Step in the Reaction of Zerovalent Iron with Water. *J. Chem. Theory Comput.* **2011**, *7*, 2876−2885.

(32) DeYonker, N. J.; Peterson, K. A.; Steyl, G.; Wilson, A. K.; Cundari, T. R. Quantitative Computational Thermochemistry of Transition Metal Species. *J. Phys. Chem. A* **2007**, *111*, 11269−11277.

(33) Perdew, J. P.; Wang, Y. Accurate and Simple Analytic Representation of the Electron-Gas Correlation-Energy. *Phys. Rev. B* **1992**, *45*, 13244−13249.

(34) Hamprecht, F. A.; Cohen, A. J.; Tozer, D. J.; Handy, N. C. Development and Assessment of New Exchange-Correlation Functionals. *J. Chem. Phys.* **1998**, *109*, 6264−6271.

(35) Dunning, T. H. Gaussian-Basis Sets for Use in Correlated Molecular Calculations. 1. The Atoms Boron through Neon and Hydrogen. *J. Chem. Phys.* **1989**, *90*, 1007−1023.

(36) Balabanov, N. B.; Peterson, K. A. Systematically Convergent Basis Sets for Transition Metals. I. All-electron Correlation Consistent Basis Sets for the 3d Elements Sc-Zn. *J. Chem. Phys.* **2005**, *123*, 064107.
(37) Frisch, M. J.; et al. *Gaussian 09*, revision A.02; Gaussian, Inc.: Wallingford, CT, 2009.
(38) Karlicky, F.; Otyepka, M.; Schroeder, D. Ligand Effects on Single-Electron Transfer of Isolated Iron Atoms in the Gaseous Complexes $[(OC)_mFe(OH_2)_n]^+$ (m, n = 0−2, m + n = 1, 2). *Int. J. Mass Spectrom.* **2012**, *330*−*332*, 95−99.
(39) Eshuis, H.; Bates, J. E.; Furche, F. Electron Correlation Methods Based on the Random Phase Approximation. *Theor. Chem. Acc.* **2012**, *131*, 1084.
(40) Ren, X. G.; Rinke, P.; Joas, C.; Scheffler, M. Random-Phase Approximation and its Applications in Computational Chemistry and Materials Science. *J. Mater. Sci.* **2012**, *47*, 7447−7471.
(41) Blochl, P. E. Projector Augmented-Wave Method. *Phys. Rev. B* **1994**, *50*, 17953−17979.
(42) Kresse, G.; Joubert, D. From Ultrasoft Pseudopotentials to the Projector Augmented-Wave Method. *Phys. Rev. B* **1999**, *59*, 1758−1775.
(43) Perdew, J. P.; Burke, K.; Ernzerhof, M. Generalized Gradient Approximation Made Simple (vol 77, pg 3865, 1996). *Phys. Rev. Lett.* **1997**, *78*, 1396.
(44) Lazar, P.; Otyepka, M. Dissociation of Water on Iron Surfaces: Generalized Gradient Functional and Range-Separated Hybrid Functional Study. *J. Phys. Chem. C* **2012**, *116*, 25470−25477.
(45) Kauffman, J. W.; Hauge, R. H.; Margrave, J. L. Studies of Reactions of Atomic and Diatomic Cr, Mn, Fe, Co, Ni, Cu, and Zn with Molecular Water at 15-K. *J. Phys. Chem.* **1985**, *89*, 3541−3547.
(46) Zhang, L. N.; Zhou, M. F.; Shao, L. M.; Wang, W. N.; Fan, K. N.; Qin, Q. Z. Reactions of Fe with H_2O and FeO with H_2. A Combined Matrix Isolation FTIR and Theoretical Study. *J. Phys. Chem. A* **2001**, *105*, 6998−7003.
(47) Stanton, J. F. On the Extent of Spin Contamination in Open-Shell Coupled-Cluster Wave-Functions. *J. Chem. Phys.* **1994**, *101*, 371−374.
(48) Jiang, W. Y.; DeYonker, N. J.; Wilson, A. K. Multireference Character for 3d Transition-Metal-Containing Molecules. *J. Chem. Theory Comput.* **2012**, *8*, 460−468.
(49) Patchkovskii, S.; Ziegler, T. Improving "Difficult" Reaction Barriers with Self-Interaction Corrected Density Functional Theory. *J. Chem. Phys.* **2002**, *116*, 7806−7813.
(50) Vydrov, O. A.; Scuseria, G. E. Effect of the Perdew-Zunger Self-Interaction Correction on the Thermochemical Performance of Approximate Density Functionals. *J. Chem. Phys.* **2004**, *121*, 8187−8193.
(51) Baerends, E. J.; Branchadell, V.; Sodupe, M. Atomic Reference Energies for Density Functional Calculations. *Chem. Phys. Lett.* **1997**, *265*, 481−489.
(52) Eder, M.; Terakura, K.; Hafner, J. Initial Stages of Oxidation of (100) and (110) Surfaces of Iron Caused by Water. *Phys. Rev. B* **2001**, *64*, 115426.
(53) Hung, W. H.; Schwartz, J.; Bernasek, S. L. Sequential Oxidation of Fe(100) by Water-Adsorption: Formation of an Ordered Hydroxylated Surface. *Surf. Sci.* **1991**, *248*, 332−342.
(54) Feibelman, P. J.; Hammer, B.; Norskov, J. K.; Wagner, F.; Scheffler, M.; Stumpf, R.; Watwe, R.; Dumesic, J. The CO/Pt(111) Puzzle. *J. Phys. Chem. B* **2001**, *105*, 4018−4025.
(55) Binnie, S. J.; Sola, E.; Alfe, D.; Gillan, M. J. Benchmarking DFT Surface Energies with Quantum Monte Carlo. *Mol. Simul.* **2009**, *35*, 609−612.
(56) Stroppa, A.; Termentzidis, K.; Paier, J.; Kresse, G.; Hafner, J. CO Adsorption on Metal Surfaces: A Hybrid Functional Study with Plane-Wave Basis Set. *Phys. Rev. B* **2007**, *76*, 195440.
(57) Harl, J.; Kresse, G. Accurate Bulk Properties from Approximate Many-Body Techniques. *Phys. Rev. Lett.* **2009**, *103*, 056401.
(58) Gruneis, A.; Marsman, M.; Harl, J.; Schimka, L.; Kresse, G. Making the Random Phase Approximation to Electronic Correlation Accurate. *J. Chem. Phys.* **2009**, *131*, 154115.
(59) Ren, X. G.; Tkatchenko, A.; Rinke, P.; Scheffler, M. Beyond the Random-Phase Approximation for the Electron Correlation Energy: The Importance of Single Excitations. *Phys. Rev. Lett.* **2011**, *106*, 153003.
(60) Hesselmann, A.; Gorling, A. Correct Description of the Bond Dissociation Limit without Breaking Spin Symmetry by a Random-Phase-Approximation Correlation Functional. *Phys. Rev. Lett.* **2011**, *106*, 093001.
(61) Olsen, T.; Thygesen, K. S. Extending the Random-Phase Approximation for Electronic Correlation Energies: The Renormalized Adiabatic Local Density Approximation. *Phys. Rev. B* **2012**, *86*, 081103.